Dynamically Switching the Polarization State of Light Based on the Phase Transition of Vanadium Dioxide

Zhi-Yong Jia,[1] Fang-Zhou Shu,[1] Ya-Jun Gao,[1] Feng Cheng,[2] Ru-Wen Peng,[1,*] Ren-Hao Fan,[1] Yongmin Liu,[2,3,†] and Mu Wang[1,‡]

[1]*National Laboratory of Solid State Microstructures, School of Physics, and Collaborative Innovation Center of Advanced Microstructures, Nanjing University, Nanjing 210093, China*
[2]*Department of Electrical and Computer Engineering, Northeastern University, Boston, Massachusetts 02115, USA*
[3]*Department of Mechanical and Industrial Engineering, Northeastern University, Boston, Massachusetts 02115, USA*

There have been great endeavors devoted to manipulating the polarization state of light by plasmonic nanostructures in recent decades. However, the topic of active polarizers has attracted much less attention. We present a composite plasmonic nanostructure consisting of vanadium dioxide that can dynamically modulate the polarization state of the reflected light through a thermally induced phase transition of vanadium dioxide. We design a system consisting of anisotropic plasmonic nanostructures with vanadium dioxide that exhibits distinct reflections subjected to different linearly polarized incidence at room temperature and in the heated state. Under a particular linearly polarized incidence, the polarization state of the reflected light changes at room temperature, and reverts to its original polarization state above the phase-transition temperature. The composite structure can also be used to realize a dynamically switchable infrared image, wherein a pattern can be visualized at room temperature while it disappears above the phase-transition temperature. The composite structure could be potentially used for versatile optical modulators, molecular detection, and polarimetric imaging.

I. INTRODUCTION

Manipulating the polarization state of light is important in numerous electromagnetic and photonic applications. Traditionally, polarization control is realized by passing light through birefringent materials that present different refractive indexes for differently polarized light. However, the volume of the polarizers is too large to integrate within on-chip nanophotonic devices. Recently, plasmonic polarizers have attracted widespread attention thanks to their compactness and design flexibility [1]. Various polarizers, such as half- and quarter-wave plates, have been designed by means of anisotropic nanostructures at visible [2–4], infrared [5–9], terahertz [10,11], and microwave wavelengths [12]. Although most of these polarizers function over narrow wavelength ranges owing to the intrinsic dispersion of the metallic nanostructures, the dispersion can be canceled out by combining the plasmonic nanostructures with a dielectric layer [7–11].

Thus far, the majority of the demonstrated plasmonic nanostructures have been in solid state, implying that it is difficult to dynamically tune the polarization state of light once these structures are fabricated. Developing active polarizers can diversify the functions of polarizers. Recently, tunable nanophotonic devices have drawn intense attention, with great promise for practical applications [13,14]. Tunable plasmonic devices have been realized by integrating plasmonic nanostructures with active media such as liquid crystals [15,16], transparent conducting oxides [17,18], graphene [19–21], and phase-transition materials [22–25]. With these materials, tunable amplitude, phase, and resonance frequency have been achieved by changing the voltage or temperature.

However, only a few studies have been conducted to achieve active polarizers [11,21]. One recent work from our group realized a freely tunable broadband polarization rotator for terahertz waves [11]. In this paper, we combine plasmonic nanostructures and vanadium dioxide (VO_2) to dynamically tune the polarization state of the reflected light. VO_2 has been extensively researched for several

*Corresponding author.
rwpeng@nju.edu.cn
†Corresponding author.
y.liu@northeastern.edu
‡Corresponding author.
muwang@nju.edu.cn

decades. It undergoes an insulator-metal transition above 68 °C, accompanied by a structural transition from the monoclinic phase to the rutile one [22,26].

The mechanism for such an insulator-metal transition is still under debate [27]. It is generally accepted that the transition might originate from the Mott transition associated with electron-electron correlations or the Peierls transition involving electron-phonon interactions [26,28]. Nevertheless, the phase transition can induce a large change in the refractive index of VO_2, which is several orders of magnitude higher than the achievable index modulation via the typical nonlinear effect [29,30]. VO_2 has previously been explored for memory meta-materials [31], involving the insulator-metal transition induced by a terahertz electric field [32], tunable reflection and transmission [33], and intelligent windows [34]. Interestingly, the phase transition of VO_2 can also be triggered by light [35,36] and electrical current [37,38]. For example, the ultrafast dynamics of photo-induced insulator-to-metal transitions makes VO_2 a promising candidate for all-optical control devices.

In this work, we present a composite plasmonic nano-structure with VO_2 that can dynamically modulate the polarization state of the reflected light via thermally induced phase transition of VO_2. First, we design aniso-tropic plasmonic nanostructures with VO_2 and investigate the changes in the reflection and absorption characteristics under *x*- and *y*-polarized incidence upon heating the sample. Then we confirm the experimental results through simulations and discuss the mechanism of modulation. Next, based on the differences between the light modula-tion under *x*- and *y*-polarized incidence, we demonstrate that the polarization state of the reflected light under particular linearly polarized incidence can be dynamically tuned by changing temperatures. Finally, we design a pattern based on the composite nanostructure to realize a dynamically switchable infrared image, where the pattern can be visualized at room temperature, while it disappears above the phase-transition temperature.

II. STRUCTURE DESIGN AND FABRICATION

The configuration of the composite plasmonic nano-structure with VO_2 is illustrated in Fig. 1(a). It consists of four layers: the lowest layer is a gold (Au) film, with a silicon dioxide (SiO_2) layer on top of it. Above these are two types of periodic gold particles in the shapes of the letters L and l. Finally, the whole sample is covered with a VO_2 layer. In the experiments, the sample is fabricated as follows. First, a 100-nm-thick gold film and a 150-nm-thick SiO_2 layer are successively deposited onto a glass substrate using magnetron sputtering. Then, periodic L and l particle arrays are defined using standard electron beam lithography followed by a gold lift-off procedure. The lengths of the L particles along the *x* and *y* directions are 300 and 170 nm, respectively, whereas the length of the l particles is 300 nm.
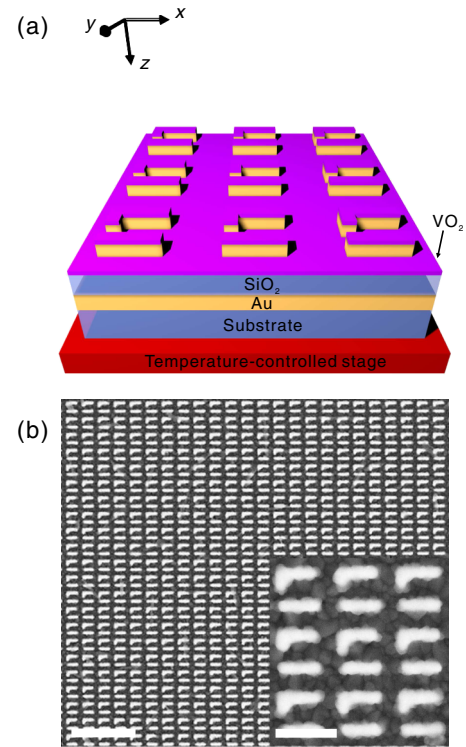

FIG. 1. (a) Schematic of the dynamically switchable polarizer. The structure consists of a periodic array of gold particles in the shapes of L and l. SiO_2 and Au films are situated below the array, whereas the VO_2 film covers the array. Glass is used as the substrate. The sample is placed on a temperature-controlled stage. (b) SEM image of the sample after covering it with VO_2; the scale bar is 1600 nm. (Inset) High-magnification SEM image; the scale bar is 400 nm.

The width and the thickness of the L and l particles are both 50 nm. The gap between the L and l particles is 100 nm, and the periods along both the *x* and *y* directions are 400 nm. Next, a 25-nm-thick vanadium film is deposited on the sample using electron-gun evaporation. Finally, the vana-dium film is transformed into a 50-nm-thick VO_2 film by thermally annealing it for 150 min under an oxygen atmosphere at 450 °C and 10 Pa pressure. Figure 1(b) shows a scanning electron microscope (SEM) image of the final sample after covering it with VO_2. An array of regular L and l particles periodically arranged in two perpendicular directions is clearly observed. The small shape discrepancy of the L and l particles is due to the inhomogeneous growth of VO_2.

III. RESULTS AND DISCUSSION

A. Reflection and absorption modulation under the *x*-polarized incidence

We measure the optical properties of the fabricated sample at different temperatures under *x*- and *y*-polarized incidence. The sample is placed on a temperature-controlled stage, and the reflection spectra of the sample

are measured in the range of 0.65 to 1.6 μm at different temperatures, using a UV-visible-near-infrared microspectrophotometer (CRAIC QDI2010), whereas the reflection spectra of the sample in the range of 1.6 to 6 μm are measured using a Fourier-transform infrared spectrometer (Vertex 70v, Bruker) combined with an infrared microscope equipped with a focal plane array (FPA) detector (Hyperion 3000, Bruker). Figure 2(a) shows the reflection spectra of the sample at 20 °C and 80 °C, under the x-polarized incidence. At 20 °C, there are two reflection dips, at 1.08 and 4.5 μm. There are also two reflection dips at 80 °C, but they are located at 0.75 and 3.08 μm, respectively. The reflection at 1.08 μm is 15% at 20 °C, and it increases to 50% at 80 °C. In addition, the reflection at 4.5 μm is 17% at 20 °C, and it increases to 74% at 80 °C. Thus, it is evident that the reflection around the two wavelengths can be modulated through the thermally induced phase transition of VO$_2$.

Figure 2(b) presents the absorption spectra of the sample at 20 °C and 80 °C under the x-polarized incidence. The absorption (A) is obtained based on the relationship $A = 1 - R - T$, where R and T denote the reflection and the transmission, respectively. Because of the presence of a reflective gold mirror, the transmission is zero in the wavelength range considered. As shown in Fig. 2(b), the absorption at 1.08 μm is 85% at 20 °C, and it decreases to 50% at 80 °C. In addition, the absorption at 4.5 μm is 83% at 20 °C, and it decreases to 26% at 80 °C. Therefore, the absorption at the two wavelengths can also be modulated by the thermally induced phase transition of VO$_2$. It means

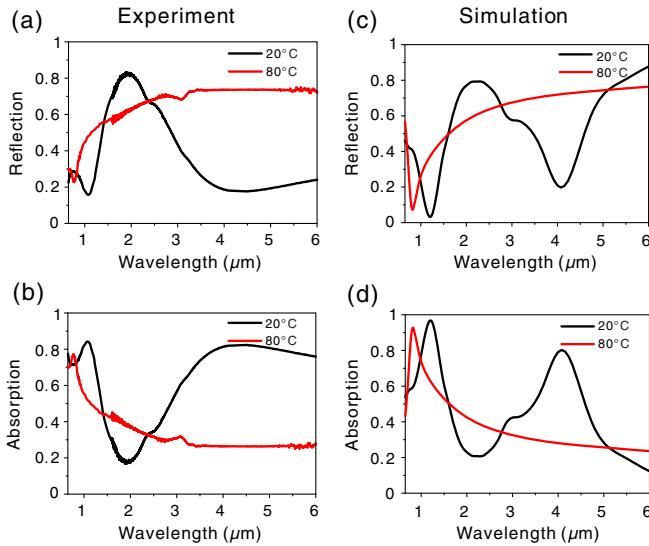that we also demonstrate a tunable absorber by integrating plasmonic nanostructures with VO$_2$.

To further confirm the above experimental results, we simulate the optical properties of the sample using the finite-difference-time-domain software FDTD Solutions from Lumerical Solutions. The complex refractive index data of VO$_2$ in the metallic and dielectric phases are taken from the literature [29], whereas the complex refractive index data for Au are interpolated from the literature data [39]. Figure 2(c) shows the calculated reflection spectra of the sample at 20 °C and 80 °C under the x-polarized incidence. There are two reflection dips, at the wavelengths of 1.2 and 4.1 μm, at 20 °C, which is in good agreement with the experimental results. However, there is only a single reflection dip, at 0.8 μm, at 80 °C. The calculated reflection of the sample at 1.2 μm is 3% at 20 °C, and it increases to 38% at 80 °C. In addition, the calculated reflection of the sample at 4.1 μm is 20% at 20 °C, and it increases to 72% at 80 °C. The wavelengths and intensities of the reflection dips at 20 °C and 80 °C slightly deviate from the experimental results. These discrepancies are ascribed to the imperfections in the fabricated sample, as well as the difference between the refractive index of VO$_2$ in our sample and the corresponding literature data. Figure 2(d) presents the calculated absorption spectra of the sample at 20 °C and 80 °C under the x-polarized incidence. Similar to the previous experimental results, the absorption at 1.2 μm is 97% at 20 °C, and it decreases to 62% at 80 °C. In addition, the absorption at 4.1 μm is 80% at 20 °C, and it decreases to 28% at 80 °C.

In order to understand the modulation in the reflection and absorption spectra under the x-polarized incidence, we analyze the electric-field distribution at these resonance wavelengths. Figures 3(a) and 3(b) show the electric-field distribution for VO$_2$ in the dielectric state at 1.2 μm in the x-y and x-z planes, respectively. It is observed that the electric field is focused mainly on the edges of the L particle

FIG. 2. (a),(b) Experimental reflection and absorption spectra of the sample for VO$_2$ in the dielectric state (at 20 °C) and the metallic state (at 80 °C), respectively, under the x-polarized incidence. (c),(d) Simulated reflection and absorption spectra of the sample for VO$_2$ in the dielectric and metallic states, respectively, under the x-polarized incidence.
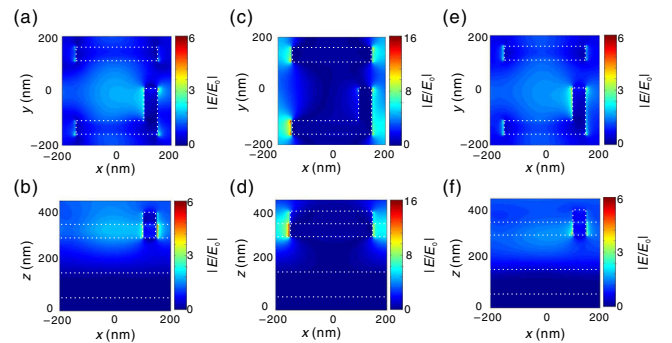

FIG. 3. (a),(c),(e) Calculated in-plane electric-field distributions of the sample at 1.2, 4.1, and 0.8 μm, respectively, under the x-polarized incidence. (b),(d),(f) Calculated vertical cross-section electric-field distributions of the sample at 1.2, 4.1, and 0.8 μm, respectively, under the x-polarized incidence. The data in (a)–(d) are for VO$_2$ in the dielectric state, whereas those in (e) and (f) are for VO$_2$ in the metallic state.

owing to the localized surface plasmon of the L particle [40]. The field localization leads to a dip in the reflection spectrum and a peak in the absorption spectrum.

Figures 3(c) and 3(d) present the electric-field distribution for VO_2 in the dielectric state at 4.1 μm in the x-y and x-z planes, respectively. The electric field is concentrated mainly between the gap of two neighboring L particles and between the gap of two neighboring I particles along the x axis; which results from the strong coupling between two neighboring L particles and the strong coupling between two neighboring I particles [41]. The field concentration also results in a dip in the reflection spectrum and a peak in the absorption spectrum.

Figures 3(e) and 3(f) exhibit the electric-field distributions for VO_2 in the metallic state at 0.8 μm in the x-y and x-z planes, respectively. Similar to the resonance at 1.2 μm for VO_2 in the dielectric state, the electric field is focused mainly on the edges of the L particle, which originates from the localized surface plasmon of the L particle. However, owing to the lower refractive index of VO_2 in the metallic phase compared to the dielectric phase [29], the dip in the reflection spectrum and the peak in the absorption spectrum shift from 1.2 to 0.8 μm.

However, there is no dip in the reflection spectrum or peak in the absorption spectrum for VO_2 in the metallic state similar to the resonance at 4.1 μm for VO_2 in the dielectric state, which is due to the "shortness" of neighboring L particles and of neighboring I particles [42], and thus there is no strong coupling between the neighboring L particles or strong coupling between neighboring I particles. Therefore, because of the insulator-metal transition, the refractive index of VO_2 has significantly changed, which eventually modulates the reflection and absorption spectra under the x-polarized incidence.

B. Reflection and absorption modulation under the *y*-polarized incidence

Now we discuss the reflection spectra of the sample at 20 °C and 80 °C under the y-polarized incidence. As shown in Fig. 4(a), at 20 °C, there are three reflection dips, at 1.25, 2.3, and 3.1 μm, respectively. However, at 80 °C, there are two reflection dips, at 1.05 and 3.08 μm. The reflection at 1.05 μm is 56% at 20 °C, and it decreases to 24% at 80 °C. On the contrary, the reflection at 3.1 μm is 6.6% at 20 °C, and it increases to 58% at 80 °C. Therefore, we can modulate the reflection in the vicinity of these two wavelengths through the thermally induced phase transition of VO_2. In addition, owing to the opposing natures of the modulations around the two wavelengths, the structure can also be considered a tunable filter for reflected light. When VO_2 is in the dielectric state, the shorter wavelength light can be reflected, whereas the longer wavelength is filtered. By contrast, when VO_2 is in the metallic state, the shorter wavelength is filtered, while the longer wavelength can be reflected.
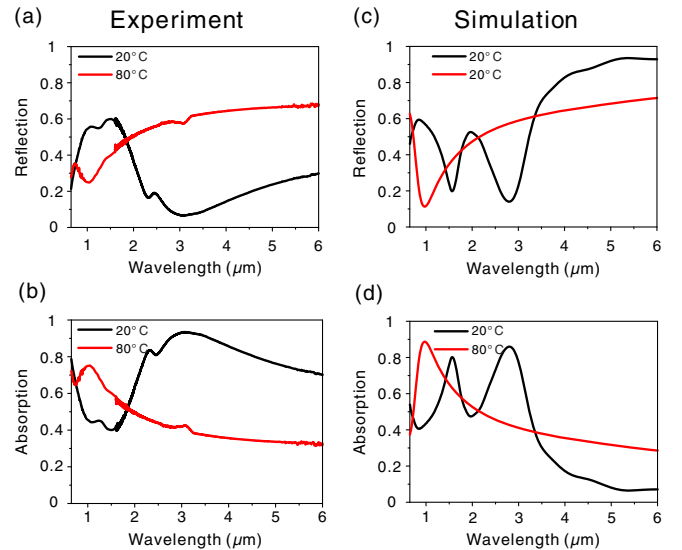

FIG. 4. (a),(b) Experimental reflection and absorption spectra of the sample for VO_2 in the dielectric state (at 20 °C) and the metallic state (at 80 °C), respectively, under the y-polarized incidence. (c),(d) Simulated reflection and absorption spectra of the sample for VO_2 in the dielectric and metallic states, respectively, under the y-polarized incidence.

Figure 4(b) presents the experimental absorption spectra of the sample at 20 °C and 80 °C under the y-polarized incidence. We can observe that the absorption at 3.1 μm is 93.4% at 20 °C, and it decreases to 42% at 80 °C. On the contrary, the absorption at 1.05 μm is 44% at 20 °C, and it increases to 76% at 80 °C. Thus, we can modulate the absorption around the two wavelengths through the thermally induced phase transition of VO_2.

The calculated reflection spectra of the sample at 20 °C and 80 °C under the y-polarized incidence are presented in Fig. 4(c). There are two reflection dips, at 1.6 and 2.85 μm, at 20 °C, and one reflection dip, at 1 μm, at 80 °C. However, the reflection dips at 20 °C and 80 °C deviate slightly from the experimental results, and there is no reflection dip at 2.3 μm at 20 °C, which might be due to the imperfections in the fabricated sample and the difference between the refractive index of VO_2 in our sample and the corresponding literature data, as we have discussed.

Figure 4(d) presents the calculated absorption spectra of the sample at 20 °C and 80 °C under the y-polarized incidence. Similar to the previous experimental results, the absorption at 2.85 μm is 86% at 20 °C, and it decreases to 43% at 80 °C. On the contrary, the absorption at 1 μm is 43% at 20 °C, and it increases to 89% at 80 °C.

In order to understand the modulation in the reflection and absorption spectra under the y-polarized incidence, we analyze the electric-field distribution at these resonance wavelengths. Figures 5(a) and 5(b) show the electric-field distribution for VO_2 in the dielectric state at 1.6 μm in the x-y and y-z planes, respectively. As observed, the electric field is focused mainly on the edges of the L particle owing
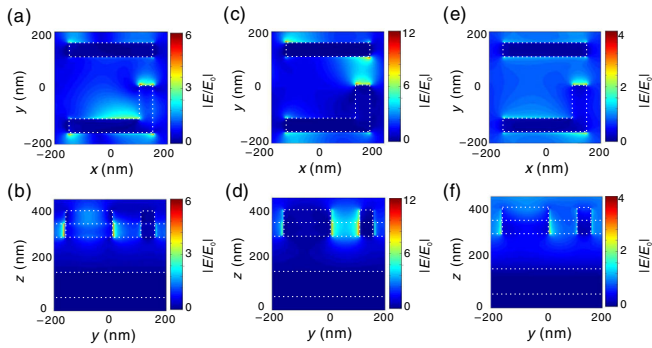
FIG. 5.   (a),(c),(e) Calculated in-plane electric-field distributions of the sample at 1.6, 2.85, and 1 μm, respectively, under the y-polarized incidence. (b),(d),(f) Calculated vertical cross-section electric-field distributions of the sample at 1.6, 2.85, and 1 μm, respectively, under the y-polarized incidence. The data in (a)–(d) are for VO_2 in the dielectric state, whereas those in (e) and (f) are for VO_2 in the metallic state.

to the localized surface plasmon of the L particle. The field localization leads to a dip in the reflection spectrum and a peak in the absorption spectrum. Figures 5(c) and 5(d) present the electric-field distribution for VO_2 in the dielectric state at 2.85 μm in the x-y and y-z planes, respectively. The electric field concentrates mainly on the gap between the L and I particles, which results from the strong coupling between the L and I particles. The field concentration also leads to a dip in the reflection spectrum and a peak in the absorption spectrum. Figures 5(e) and 5(f) reveal the electric-field distribution for VO_2 in the metallic state at 1 μm in the x-y and y-z planes, respectively. Similar to the resonance at 1.6 μm for VO_2 in the dielectric state, the electric field is mainly on the edges of the L particle, which originates from the localized surface plasmon of the L particle. However, as a result of the lower refractive index of VO_2 in the metallic phase compared to the dielectric phase, the dip in the reflection spectrum and the peak in the absorption spectrum shift from 1.6 to 1 μm. By contrast, there is no dip in the reflection spectrum or peak in the absorption spectrum for VO_2 in the metallic state similar to the resonance at 2.85 μm for VO_2 in the dielectric state, which is due to the "shortness" between the L and I particles when VO_2 is in the metallic state, and thus there is no strong coupling between the L and I particles. Therefore, it is the variation of the refractive index of VO_2 caused by the insulator-metal transition that modulates the reflection and absorption spectra under the y-polarized incidence.

C. Dynamically switchable polarizer

Earlier in the paper, we discuss the variation in the reflection spectra of the sample at different temperatures under x- and y-polarized incidence. Because the sample is anisotropic, the reflection spectra are different under the x- and y-polarized incidences. The reflection spectra vary

when the temperature changes because of the phase transition of VO_2. Owing to the differences in the variation of the reflection spectra with temperature between the x- and y-polarized incidences, the sample can be used as an active polarizer. For example, the reflections of the sample at 20 °C under x- and y-polarized incidence at the wavelength of 3 μm are 43% and 6.8%, respectively. However, the reflections at 80 °C under x- and y-polarized incidence at 3 μm are 68% and 58%, respectively. Therefore, if the incident light is polarized along the 135° direction, the reflected light is polarized approximately along the 0° (180°) direction at 20 °C and the 135° direction at 80 °C.

To confirm the concept of the active polarizer, we fix the polarization of the incident light along the 135° direction and measure the reflection spectra of the sample at 3 μm wavelength and different analyzer angles in the range of 0° to 180° in steps of 15° at 20 °C and 80 °C. As shown in Fig. 6(a), the highest reflection is observed for polarization along the 165° direction at 20 °C, and the lowest reflection is observed near 0 for polarization along the 75° direction at 20 °C. Therefore, the polarization of the reflected light is approximately along the 165° direction at 20 °C.

However, the highest reflection is observed for polarization along the 135° direction at 80 °C, and the lowest reflection is observed near 0 for polarization along the 45° direction at 80 °C. Therefore, the polarization of the reflected light is approximately along the 135° direction at 80 °C. Remarkably, the phase transition of VO_2 is reversible; hence, the polarization of the reflected light reverts to the 165° direction when the temperature is decreased to room temperature.

As shown in Fig. 6(b), at 20 °C, the polarization of the reflected light is along the 165° direction, but it is changed to the 135° direction if the temperature increases to 80 °C. Once the temperature decreases to 20 °C, it reverts to the 165° direction. Therefore, the polarization of the reflected

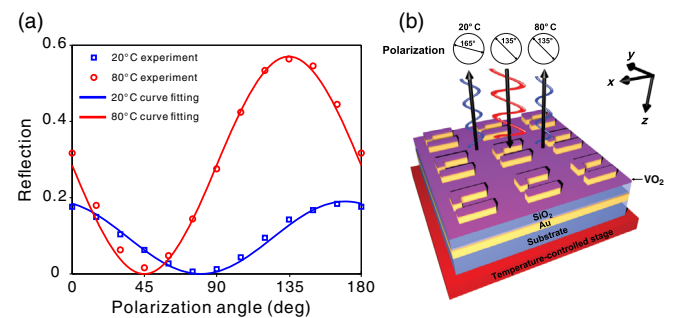FIG. 6.   (a) Experimental reflection spectra of the sample at 3 μm as a function of the analyzer angle at 20 °C and 80 °C when the incident linear polarization is along the 135° direction. (b) Schematic of the dynamically switchable polarizer: When the polarization of the incident light is along the 135° direction, the polarization of the reflected light is along the 165° direction at 20 °C, whereas it is along the 135° direction at 80 °C.

light can be switched dynamically by increasing or decreasing the temperature.

The experimental data are also fitted according to Malus's law. Evidently, the experimental data match the fitting curves in Fig. 6(a) very well, further indicating that the reflected light is linearly polarized at 20 °C and 80 °C. Although we consider the polarization of the incident light only along the 135° direction, the polarization of the reflected light can also be tuned by changing the temperatures at other angles of incident polarization. For example, if the polarization of the incident light is along the 60° direction, the polarization of the reflected light is approximately along the 0° (180°) direction at 20 °C, whereas it is along the 60° direction at 80 °C. In addition, although we demonstrate the dynamically switchable polarizer at 3 μm, it is possible to adjust the geometrical parameters to realize the actively switchable polarizer at other wavelengths.

D. Dynamically switchable infrared image

Since the differences in the reflection of the sample between the *x*- and *y*-polarized incidences at 3 μm are large at 20 °C while small at 80 °C, we can realize a dynamically switchable infrared image based on the composite nanostructure. In order to confirm this concept, we designed an NJU pattern where the regions within and outside NJU are composed of two mutually perpendicular arrays with the same parameters as those of the structure shown in Fig. 1(b). The array within the region NJU under the *x*-polarized incidence is equivalent to the array outside this region under the *y*-polarized incidence. The FPA image of the sample is measured at the wavelength of 3 μm at 20 °C

(a)   20 °C

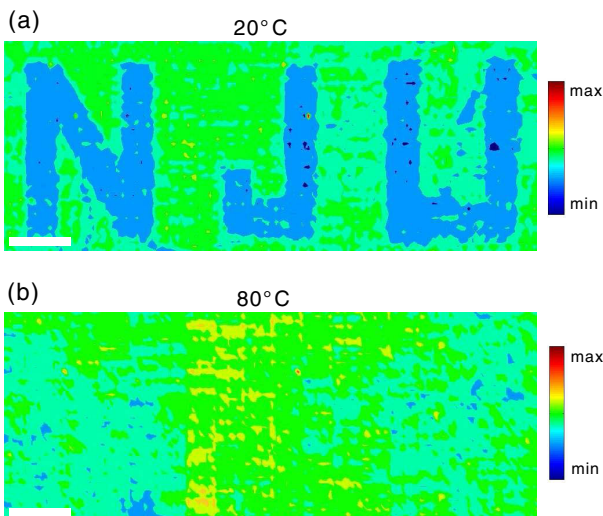(b)   80 °C

FIG. 7.   (a),(b) FPA images of a sample with an NJU pattern at the wavelength of 3 μm under the *x*-polarized incidence at 20 °C and 80 °C, respectively, where the regions within and outside NJU are composed of two mutually perpendicular arrays with the same parameters as those of the structure shown in Fig. 1(b); the scale bar is 40 μm.

and 80 °C under the *x*-polarized incidence, as shown in Figs. 7(a) and 7(b), respectively. Since the difference in the reflection between the region within NJU and that outside NJU at 3 μm is large at 20 °C under the *x*-polarized incidence, we can observe the NJU pattern in the FPA image, as presented in Fig. 7(a). However, the reflection between the region within NJU and that outside NJU at 3 μm is almost the same at 80 °C under the *x*-polarized incidence; therefore, we cannot visualize the NJU pattern in the FPA image [Fig. 7(b)]. As a result, we can dynamically switch the infrared image by changing the temperature.

IV. CONCLUSION

In conclusion, we demonstrate in this paper a dynamically switchable polarizer by integrating plasmonic nanostructures along with VO$_2$, and by exploiting the insulator-metal phase transition of the latter. Under a particular linearly polarized incidence, the polarization state of the reflected light changes at room temperature and reverts to its original polarization state above the phase-transition temperature. The composite structure can also be used to realize a dynamically switchable infrared image, where a pattern can be visualized at room temperature, whereas it disappears above the phase-transition temperature. Apart from the tunable linearly polarized light, it would be possible to use the same structure to tune the circularly polarized light [43], given its geometry symmetry. Although the polarization state changes with a relatively long response time, which is a typical diffusion-related feature, it may change much faster with the introduction of electrical current or light [35–38]. We anticipate that the fabricated composite structure could lead to many applications, such as optical modulators, molecular detection, and polarimetric imaging on a fully integrated platform.

ACKNOWLEDGMENTS

[1] H.-T. Chen, A. J. Taylor, and N. Yu, A review of metasurfaces: Physics and applications, Rep. Prog. Phys. **79,** 076401 (2016).

[2] A. Drezet, C. Genet, and T. W. Ebbesen, Miniature Plasmonic Wave Plates, Phys. Rev. Lett. **101,** 043902 (2008).

[3] J. Hao, Q. Ren, Z. An, X. Huang, Z. Chen, M. Qiu, and L. Zhou, Optical metamaterial for polarization control, Phys. Rev. A **80,** 023807 (2009).

[4] Y. Zhao and A. Alù, Manipulating light polarization with ultrathin plasmonic metasurfaces, Phys. Rev. B **84,** 205428 (2011).

[5] N. Yu, F. Aieta, P. Genevet, M. A. Kats, Z. Gaburro, and F. Capasso, A broadband, background-free quarter-wave plate based on plasmonic metasurfaces, Nano Lett. **12,** 6328 (2012).

[6] A. Pors, M. G. Nielsen, and S. I. Bozhevolnyi, Broadband plasmonic half-wave plates in reflection, Opt. Lett. **38,** 513 (2013).

[7] Q. Lévesque, M. Makhsiyan, P. Bouchon, F. Pardo, J. Jaeck, N. Bardou, C. Dupuis, R. Haïdar, and J.-L. Pelouard, Plasmonic planar antenna for wideband and efficient linear polarization conversion, Appl. Phys. Lett. **104,** 111105 (2014).

[8] S.-C. Jiang, X. Xiong, Y.-S. Hu, Y.-H. Hu, G.-B. Ma, R.-W. Peng, C. Sun, and M. Wang, Controlling the Polarization State of Light with a Dispersion-Free Metastructure, Phys. Rev. X **4,** 021026 (2014).

[9] F. Ding, Z. Wang, S. He, V. M. Shalaev, and A. V. Kildishev, Broadband high-efficiency half-wave plate: A supercell-based plasmonic metasurface approach, ACS Nano **9,** 4111 (2015).

[10] N. K. Grady, J. E. Heyes, D. R. Chowdhury, Y. Zeng, M. T. Reiten, A. K. Azad, A. J. Taylor, D. A. R. Dalvit, and H.-T. Chen, Terahertz metamaterials for linear polarization conversion and anomalous refraction, Science **340,** 1304 (2013).

[11] R.-H. Fan, Y. Zhou, X.-P. Ren, R.-W. Peng, S.-C. Jiang, D.-H. Xu, X. Xiong, X.-R. Huang, and M. Wang, Freely tunable broadband polarization rotator for terahertz waves, Adv. Mater. **27,** 1201 (2015).

[12] J. Hao, Y. Yuan, L. Ran, T. Jiang, J. A. Kong, C. T. Chan, and L. Zhou, Manipulating Electromagnetic Wave Polarization by Anisotropic Metamaterials, Phys. Rev. Lett. **99,** 063908 (2007).

[13] N. I. Zheludev and Y. S. Kivshar, From metamaterials to metadevices, Nat. Mater. **11,** 917 (2012).

[14] Z. Wang, L. Jing, K. Yao, Y. Yang, B. Zheng, C. M. Soukoulis, H. Chen, and Y. Liu, Origami-based reconfigurable metamaterials for tunable chirality, Adv. Mater. **29,** 1700412 (2017).

[15] X. Wang, D.-H. Kwon, D. H. Werner, I.-C. Khoo, A. V. Kildishev, and V. M. Shalaev, Tunable optical negative-index metamaterials employing anisotropic liquid crystals, Appl. Phys. Lett. **91,** 143122 (2007).

[16] D. Shrekenhamer, W.-C. Chen, and W. J. Padilla, Liquid Crystal Tunable Metamaterial Absorber, Phys. Rev. Lett. **110,** 177403 (2013).

[17] Y.-W. Huang, H. W. H. Lee, R. Sokhoyan, R. A. Pala, K. Thyagarajan, S. Han, D. P. Tsai, and H. A. Atwater, Gate-tunable conducting oxide metasurfaces, Nano Lett. **16,** 5319 (2016).

[18] J. Park, J.-H. Kang, S. J. Kim, X. Liu, and M. L. Brongersma, Dynamic reflection phase and polarization control in metasurfaces, Nano Lett. **17,** 407 (2017).

[19] N. K. Emani, T.-F. Chung, X. Ni, A. V. Kildishev, Y. P. Chen, and A. Boltasseva, Electrically tunable damping of plasmonic resonances with graphene, Nano Lett. **12,** 5202 (2012).

[20] Y. Yao, M. A. Kats, P. Genevet, N. Yu, Y. Song, J. Kong, and F. Capasso, Broad electrical tuning of graphene-loaded plasmonic antennas, Nano Lett. **13,** 1257 (2013).

[21] Z. Miao, Q. Wu, X. Li, Q. He, K. Ding, Z. An, Y. Zhang, and L. Zhou, Widely Tunable Terahertz Phase Modulation with Gate-Controlled Graphene Metasurfaces, Phys. Rev. X **5,** 041027 (2015).

[22] D. W. Ferrara, J. Nag, E. R. MacQuarrie, A. B. Kaye, and R. F. Haglund, Plasmonic probe of the semiconductor to metal phase transition in vanadium dioxide, Nano Lett. **13,** 4169 (2013).

[23] A. U. Michel, P. Zalden, D. N. Chigrin, M. Wuttig, A. M. Lindenberg, and T. Taubner, Reversible optical switching of infrared antenna resonances with ultrathin phase-change layers using femtosecond laser pulses, ACS Photonics **1,** 833 (2014).

[24] A. Tittl, A. U. Michel, M. Schäferling, X. Yin, B. Gholipour, L. Cui, M. Wuttig, T. Taubner, F. Neubrech, and H. Giessen, A switchable mid-infrared plasmonic perfect absorber with multispectral thermal imaging capability, Adv. Mater. **27,** 4597 (2015).

[25] Q. Wang, E. T. F. Rogers, B. Gholipour, C.-M. Wang, G. Yuan, J. Teng, and N. I. Zheludev, Optically reconfigurable metasurfaces and photonic devices based on phase change materials, Nat. Photonics **10,** 60 (2016).

[26] Z. Yang, C. Ko, and S. Ramanathan, Oxide electronics utilizing ultrafast metal-insulator transitions, Annu. Rev. Mater. Res. **41,** 337 (2011).

[27] W. H. Brito, M. C. O. Aguiar, K. Haule, and G. Kotliar, Metal-Insulator Transition in VO_2: A DFT + DMFT Perspective, Phys. Rev. Lett. **117,** 056402 (2016).

[28] S. Chen, Z. Wang, L. Fan, Y. Chen, H. Ren, H. Ji, D. Natelson, Y. Huang, J. Jiang, and C. Zou, Sequential insulator-metal-insulator phase transitions of VO_2 triggered by hydrogen doping, Phys. Rev. B **96,** 125130 (2017).

[29] H. W. Verleur, A. S. Barker, and C. N. Berglund, Optical properties of VO_2 between 0.25 and 5 eV, Phys. Rev. **172,** 788 (1968).

[30] M. J. Dicken, K. Aydin, I. M. Pryce, L. A. Sweatlock, E. M. Boyd, S. Walavalkar, J. Ma, and H. A. Atwater, Frequency tunable near-infrared metamaterials based on VO_2 phase transition, Opt. Express **17,** 18330 (2009).

[31] T. Driscoll, H.-T. Kim, B.-G. Chae, B.-J. Kim, Y.-W. Lee, N. M. Jokerst, S. Palit, D. R. Smith, M. Di Ventra, and D. N. Basov, Memory metamaterials, Science **325,** 1518 (2009).

[32] M. Liu, H. Y. Hwang, H. Tao, A. C. Strikwerda, K. Fan, G. R. Keiser, A. J. Sternbach, K. G. West, S. Kittiwatanakul, J. Lu, S. A. Wolf, F. G. Omenetto, X. Zhang, K. A. Nelson, and R. D. Averitt, Terahertz-field-induced insulator-to-metal transition in vanadium dioxide metamaterial, Nature (London) **487,** 345 (2012).

[33] J. Rensberg, S. Zhang, Y. Zhou, A. S. McLeod, C. Schwarz, M. Goldflam, M. Liu, J. Kerbusch, R. Nawrodt, S. Ramanathan, D. N. Basov, F. Capasso, C. Ronning, and M. A. Kats, Active optical metasurfaces based on defect-engineered phase-transition materials, Nano Lett. **16,** 1050 (2016).

[34] S.-Y. Li, G. A. Niklasson, and C. G. Granqvist, Thermochromic fenestration with VO_2-based materials: Three

challenges and how they can be met, Thin Solid Films **520**, 3823 (2012).

[35] A. Cavalleri, C. Tóth, C. W. Siders, J. A. Squier, F. Ráksi, P. Forget, and J. C. Kieffer, Femtosecond Structural Dynamics in VO_2 During an Ultrafast Solid-Solid Phase Transition, Phys. Rev. Lett. **87**, 237401 (2001).

[36] J. D. Ryckman, K. A. Hallman, R. E. Marvel, R. F. Haglund, and S. M. Weiss, Ultra-compact silicon photonic devices reconfigured by an optically induced semiconductor-to-metal transition, Opt. Express **21**, 10753 (2013).

[37] M. Nakano, K. Shibuya, D. Okuyama, T. Hatano, S. Ono, M. Kawasaki, Y. Iwasa, and Y. Tokura, Collective bulk carrier delocalization driven by electrostatic surface charge accumulation, Nature (London) **487**, 459 (2012).

[38] J. Jeong, N. Aetukuri, T. Graf, T. D. Schladt, M. G. Samant, and S. S. P. Parkin, Suppression of metal-insulator transition in VO_2 by electric field-induced oxygen vacancy formation, Science **339**, 1402 (2013).

[39] P. B. Johnson and R. W. Christy, Optical constants of the noble metals, Phys. Rev. B **6**, 4370 (1972).

[40] S. A. Maier, *Plasmonics: Fundamentals and Applications* (Springer, New York, 2007).

[41] N. J. Halas, S. Lal, W.-S. Chang, S. Link, and P. Nordlander, Plasmons in strongly coupled metallic nanostructures, Chem. Rev. **111**, 3913 (2011).

[42] T. Driscoll, S. Palit, M. M. Qazilbash, M. Brehm, F. Keilmann, B.-G. Chae, S.-J. Yun, H.-T. Kim, S. Y. Cho, N. M. Jokerst, D. R. Smith, and D. N. Basov, Dynamic tuning of an infrared hybrid-metamaterial resonance using vanadium dioxide, Appl. Phys. Lett. **93**, 024101 (2008).

[43] Z. Wang, H. Jia, K. Yao, W. Cai, H. Chen, and Y. Liu, Circular dichroism metamirrors with near-perfect extinction, ACS Photonics **3**, 2096 (2016).